Symmetry breaking for transmission in a photonic waveguide coupled with two off-channel nonlinear defects

Evgeny Bulgakov,[1,2] Konstantin Pichugin,[1] and Almas Sadreev[1]
[1]*Kirensky Institute of Physics, 660036, Krasnoyarsk, Russia*
[2]*Siberian State Aerospace University, Krasnoyarsk Rabochii, 31, Krasnoyarsk, Russia*
(Received 19 July 2010; revised manuscript received 13 December 2010; published 28 January 2011)

We consider light transmission in a two-dimensional (2D) photonic crystal waveguide coupled with two identical nonlinear defects positioned symmetrically aside the waveguide. With the coupled mode theory, we show three scenarios for the transmission. The first one inherits the linear case and preserves the symmetry. In the second scenario, the symmetry is broken because of different light intensities at the defects. In the third scenario, the intensities at the defects are equal but phases of complex amplitudes are different. That results in a vortical power flow between the defects similar to the dc Josephson effect if the input power over the waveguide is applied and the defects are coupled. All of these phenomena agree well with computations based on an expansion of the electromagnetic field into optimally adapted photonic Wannier functions in a 2D photonic crystal.

DOI: 10.1103/PhysRevB.83.045109 PACS number(s): 42.70.Qs, 41.20.Jb, 42.65.Pc, 42.79.Gn

I. INTRODUCTION

It is believed that future integrated photonic circuits for ultrafast all-optical signal processing require different types of nonlinear functional elements such as switches, memory, and logic devices. Therefore, both physics and designs of such all-optical devices have attracted significant research efforts during the past two decades, and most of these studies utilize the concepts of optical switching and bistability. One of the simplest bistable optical devices that can be built up in photonic integrated circuits is a single cavity coupled with an optical waveguide or waveguides.[1] Its transmission properties depend on the intensity of incident light when the cavity is filled with a Kerr nonlinear material. If the characteristic optical wavelength greatly exceeds the size of the nonlinear cavity, it can be presented by a single isolated mode coupled with the waveguide. Thereby the system becomes equivalent to the single-level nonlinear Fano-Anderson model that describes a nonlinear impurity embedded in a continuum. The system has attracted interest over the past two decades because of analytical treatment and its generality.[2–12] On the other hand, the system can be realized in the two-dimensional photonic crystals (PhC).

For an extension of the number of nonlinear cavities (e.g., two) coupled with the PhC waveguide, one can expect, at first sight, two bistable resonances. However, the interference effects in the nonlinear system could give rise to a much more rich variety of resonance phenomena. As was recently shown in the framework of the nonlinear two-level Fano-Anderson model,[13] the resonances undergo crossing under variation of a frequency, although the cavities are different. Moreover, the resonance width could vanish to give rise to localization of the resonance state [i.e., the bound state in continuum (BSC)]. Because of the lack of the superposition principle, the BSC is displayed in the transmission as a resonance of rather unusual shape. The two different cavities composed of a Kerr-type material positioned aside the photonic waveguide, as shown in Fig. 1(a), realize the nonlinear two-level Fano-Anderson model.[13] Let us now consider the case of two identical nonlinear cavities positioned aside the waveguide at the same distances as shown in Fig. 1(a). Then the system is symmetric relative to the inversion of the y axis, as shown in Fig. 1. The system is even more simple compared to the system in which two nonlinear cavities are aligned along the waveguide considered by Maes *et al.*[14,15] That system is symmetric relative to the inversion of the x axis if equal power is injected on both sides of the coupled cavities. Maes *et al.* have shown that the reflected output power nevertheless might be different on both sides of the defects due to nonlinear effects (i.e., the symmetry of the system can be broken under the effect of input power). Finally, the phenomenon of the symmetry breaking has been developed in nonlinear optics[16–20] with the establishment of one or more asymmetric states that no longer preserve the symmetry properties of the original solution. The symmetry breaking was also found for the case of many coupled nonlinear optical cavities in ringlike architecture.[21,22]

In the linear case, both defects are excited by an input wave with the same strength. In the nonlinear case, this excitation shifts the resonance frequencies of the defects. Due to the nonlinearity, it is possible that the symmetric solution is no longer the only one at a certain input power or frequency of input electromagnetic (EM) field. Then the system can drift to a situation in which one defect is more excited than the other, and thus an asymmetric state arises because of different intensities of the EM field at the cavities. The scenario of the symmetry breaking described in Ref. 14 is shown to be realized in our case; however, it does not need application of input power to both sides of the waveguide. Moreover, we demonstrate a more fine mechanism of the symmetry breaking when the defects are excited with the equal intensities but with different phases.

II. PERTURBATION THEORY FOR THE DEFECT STATES

The light propagation in linear PhC is described by the Maxwell equations

$$\nabla \times \vec{E} = -\frac{\partial \vec{H}}{\partial t}, \quad \nabla \times \vec{H} = \frac{\partial \vec{D}}{\partial t}, \quad \vec{D}(\vec{r},t) = \epsilon_0(\vec{r})\vec{E}(\vec{r},t). \tag{1}$$

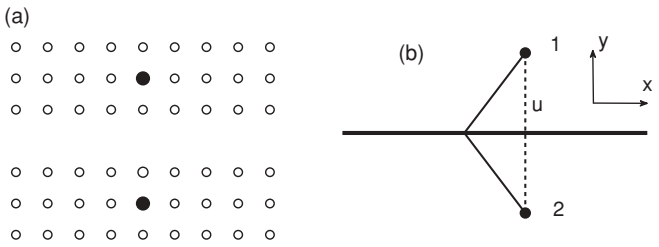

FIG. 1. (a) Two defect rods composed of a Kerr medium marked by filled circles, inserted into the square lattice photonic crystal of dielectric rods. The 1D waveguide is formed by removing of linear chain of rods. (b) Schematic system consisting of a waveguide side coupled to two single-mode cavities. The cavities are coupled each other via u.

We take the light speed $c = 1$. However, if there are defects with instantaneous Kerr nonlinearity, the displacement electric vector interior to the defects has a nonlinear contribution[23] $\vec{D}(\vec{r},t) = \epsilon_0(\vec{r})\vec{E}(\vec{r},t) + \chi^{(3)}[\vec{E}(\vec{r},t)]^2\vec{E}(\vec{r},t)$.[23,24] A substitution of the electric field in the form $[\vec{E}(\vec{r},t) = \frac{1}{2}[\vec{E}(\vec{r})e^{i\omega t} + \vec{E}^*(\vec{r})e^{-i\omega t}]$ into Eq. (1) and neglect by highly oscillating terms such as $e^{2i\omega}$ allows us to write the Maxwell equations in the same form as Eq. (1) with

$$\epsilon(\vec{r}) = \epsilon_0(\vec{r}) + \tfrac{1}{4}\chi^{(3)}(\omega)|\vec{E}(\vec{r})|^2\vec{E}(\vec{r}) + \tfrac{1}{2}\chi^{(3)}(\omega)\vec{E}^2(\vec{r})\vec{E}^*(\vec{r}). \quad (2)$$

In what follows, we consider the 2D PhC with arrays of infinitely long dielectric rods as shown in Fig. 1(a) in which the electric field is directed along the rods while the magnetic field is directed perpendicular to the rods [in the plane of Fig. 1(a)]. Then Eq. (2) simplifies as follows:[24]

$$\epsilon_0(\vec{r}) = \epsilon_0(\vec{r}) + \delta\epsilon(\vec{r}), \quad (3)$$

where $\delta\epsilon = \frac{3}{4}\chi^{(3)}(\omega)$.

If the nonlinear contribution to the dielectric constant is small, the Maxwell equation can be solved by the perturbation theory. There is a remarkable analogy of electrodynamics in dielectric media with quantum mechanics.[1,25] That allows us to use the well-known methods of quantum mechanical perturbation theory and scattering theory. Let $|\psi\rangle = \begin{pmatrix}\vec{E}\\ \vec{H}\end{pmatrix}$ be the electromagnetic state in the photonic crystal. Then the Maxwell equations (1) can be written as the Schrödinger equation $i|\dot{\psi}\rangle = \widehat{H}|\psi\rangle$ indeed with the Hamiltonian[1,25,26]

$$\widehat{H} = \begin{pmatrix} 0 & \frac{i}{\epsilon(\vec{r})}\nabla\times \\ -i\nabla\times & 0 \end{pmatrix}. \quad (4)$$

Because of the perturbation of the dielectric constant (3), the Hamiltonian can be presented as $\widehat{H} = \widehat{H}_0 + \widehat{V}$, where

$$\widehat{H}_0 = \begin{pmatrix} 0 & \frac{i}{\epsilon_0(\vec{r})}\nabla\times \\ -i\nabla\times & 0 \end{pmatrix}, \quad \widehat{V} = \begin{pmatrix} 0 & i\delta\left(\frac{1}{\epsilon(\vec{r})}\right)\nabla\times \\ 0 & 0 \end{pmatrix}, \quad (5)$$

and

$$\delta\left(\frac{1}{\epsilon(\vec{r})}\right) = \frac{1}{\epsilon(\vec{r})} - \frac{1}{\epsilon_0(\vec{r})}. \quad (6)$$

Let us introduce (following, for example, Refs. 5 and 26) the following inner product for the unperturbed system:

$$\langle\psi|\psi'\rangle = \frac{1}{2}\int[\epsilon_0(\vec{r})\vec{E}^*\vec{E}' + \vec{H}^*\vec{H}']\,d^3\vec{r}, \quad (7)$$

which obeys the following normalization and orthogonality conditions for the bound eigenstates of the unperturbed Hamiltonian $\widehat{H}_0|\psi_m\rangle = \omega_m|\psi_m\rangle$:

$$\langle\psi_n|\psi_{n'}\rangle = \frac{1}{2}\int[\epsilon_0(\vec{r})\vec{E}_n^*\vec{E}_{n'} + \vec{H}_n^*\vec{H}_{n'}]d^3\vec{r} = \int\epsilon_0(\vec{r})\vec{E}_n^*\vec{E}_{n'}d^3\vec{r} = \delta_{nn'}. \quad (8)$$

Then the matrix elements for the perturbation, calculated by the use of these eigenstates, are

$$\langle m|V|n\rangle = \frac{\omega_n}{2}\int d^3\vec{r}\,\epsilon_0^2(\vec{r})\delta\left(\frac{1}{\epsilon(\vec{r})}\right)\vec{E}_m^*(\vec{r})\vec{E}_n(\vec{r}). \quad (9)$$

One can see that the matrix (9) is not Hermitian, as was noted in Ref. 26. The reason is that the unperturbed states obey the inner product (7) with the dielectric constant $\epsilon_0(\vec{r})$, while the eigenstates of the full Hamiltonian $\widehat{H}_0 + \widehat{V}$ obey the inner product with a different dielectric constant $\epsilon(\vec{r})$. Respectively, the Hamiltonian $\widehat{H}$ is non-Hermitian with the inner product (8).

In order to avoid this problem we must use the inner product, which is not tied to a specific choice of the dielectric constant. One way, given in Ref. 1, is by using only the magnetic field for the state. Another way is to absorb the dielectric constant in the scalar product by a new function as $\vec{F} = \sqrt{\epsilon(\vec{r})}\vec{E}$. Then the inner product becomes

$$\langle\psi|\psi'\rangle = \frac{1}{2}\int(\vec{F}^*\vec{F}' + \vec{H}^*\vec{H}')\,d^3\vec{r}. \quad (10)$$

The value $\langle\psi|\psi\rangle = \frac{1}{2}\int[\epsilon(\vec{r})|\vec{E}|^2 + |\vec{H}|^2]d^3\vec{r}$ is proportional to the energy of the EM field, which is important for the derivation of the forthcoming coupled mode theory (CMT) equations. That technique changes the Maxwell equations as follows:

$$\nabla\times\frac{\vec{F}}{\sqrt{\epsilon(\vec{r})}} = -\dot{\vec{H}}, \quad \frac{1}{\sqrt{\epsilon(\vec{r})}}\nabla\times\vec{H} = \dot{\vec{F}}. \quad (11)$$

The Hamiltonian takes the following form:

$$\widehat{H}_0 = \begin{pmatrix} 0 & \frac{i}{\sqrt{\epsilon_0(\vec{r})}}\nabla\times \\ -i\nabla\times\frac{1}{\sqrt{\epsilon_0(\vec{r})}} & 0 \end{pmatrix}, \quad \widehat{V} = \begin{pmatrix} 0 & i\delta\left(\frac{1}{\sqrt{\epsilon(\vec{r})}}\right)\nabla\times \\ -i\nabla\times\delta\left(\frac{1}{\sqrt{\epsilon(\vec{r})}}\right) & 0 \end{pmatrix}. \quad (12)$$

Now the eigenstates of the full Hamiltonian can be expanded over the eigenstates $|m\rangle = \begin{pmatrix} \vec{F}_m \\ \vec{H}_m \end{pmatrix}$ of the unperturbed Hamiltonian $\widehat{H}_0$, where

$$\nabla \times \frac{\vec{F}_m}{\sqrt{\epsilon_0(\vec{r})}} = i\omega_m \vec{H}_m, \quad \nabla \times \vec{H}_m = -i\omega_m \sqrt{\epsilon_0(\vec{r})}\vec{F}_m. \tag{13}$$

Then we obtain

$$\langle m|V|n\rangle = \frac{(\omega_m + \omega_n)}{2} \int d^3\vec{r}\, \epsilon_0^{3/2}(\vec{r})\delta\left(\frac{1}{\sqrt{\epsilon(\vec{r})}}\right) E_m^*(\vec{r})E_n(\vec{r}). \tag{14}$$

One can see that the full Hamiltonian is Hermitian now.

III. COUPLED MODE THEORY OF TWO NONLINEAR DEFECTS

Let each defect support a localized nondegenerate monopole solution for the TM mode only, which has the electric field component parallel to the infinitely long rods.[1,27] Other solutions (dipole, quadrupole, etc.) are assumed to be extended in the photonic crystal for the appropriate cavity radius r_d and the dielectric constant,[27,28] and are thereby excluded from consideration. Therefore, we have a two-level description for $\widehat{H}_0$ with the eigenfrequencies

$$\omega_{s,a} = \omega_0 \mp u \tag{15}$$

if the identical defects are coupled via the coupling constant u. We denote the corresponding even (bonding) and odd (antibonding) eigenmodes as $\psi_{s,a}(\mathbf{x}), \mathbf{x} = (x,y)$, where the wave function ψ is presented by the electric field only. Both modes for specific PhC are shown in Fig. 13.

We consider that the dielectric constant $\epsilon(\mathbf{x})$ changes at the defects because of the Kerr effect

$$\epsilon_j(\mathbf{x}) = \left(\epsilon_0 + \tfrac{3}{4}\chi^{(3)}(\omega)|E(\mathbf{x})|^2\right)\theta(\mathbf{x} - \mathbf{x}_j), \quad j = 1,2. \tag{16}$$

Here j enumerates the defects, $\theta = 1$ inside the defect rod and $\theta = 0$ outside. As will be shown later (see, for example, Figs. 15 and 20), the resonance spectra in the PhC waveguide with coupled off-channel defects are located in a rather narrow frequency domain. Therefore, we neglect the frequency dependence in the nonlinear susceptibility $\chi^{(3)}(\omega)$ in the following. Assuming that the defect rods are very thin and that the nonlinear contribution in Eq. (16) is small compared to ϵ_0, we obtain for the matrix elements (14)

$$\langle m|V|n\rangle \approx -\frac{3}{16}\sigma\chi^{(3)}(\omega_m + \omega_n)\sum_{j=1,2}|E(\mathbf{x}_j)|^2\psi_m(\mathbf{x}_j)^*\psi_n(\mathbf{x}_j), \tag{17}$$

where σ is the cross section of the defects. Here we have only two eigenfunctions, the even $\psi_s(x,y) = \psi_s(x,-y)$ and the odd $\psi_a(x,y) = -\psi_a(x,-y)$, as shown in Fig. 13 with the eigenfrequencies (15). Finally, from Eq. (17), we obtain

$$\widehat{V} = \lambda \begin{pmatrix} \omega_s\phi_s^2(I_1 + I_2) & \omega_0\phi_s\phi_a(I_1 - I_2) \\ \omega_0\phi_s\phi_a(I_1 - I_2) & \omega_a\phi_a^2(I_1 + I_2) \end{pmatrix}, \tag{18}$$

where $\phi_s = \psi_s(\mathbf{x}_1)\sqrt{\sigma} = \psi_s(\mathbf{x}_2)\sqrt{\sigma}, \phi_a = \psi_a(\mathbf{x}_1)\sqrt{\sigma} = -\psi_a(\mathbf{x}_2)\sqrt{\sigma}$, $\mathbf{x}_1$ and $\mathbf{x_2}$ are the positions of the defects in the two-dimensional PhC, and $I_j = |E(\mathbf{x}_j)|^2, j = 1,2$ are the intensities of the electric field at the nonlinear defects, $\lambda = -\frac{3}{4}\chi^{(3)}$.

In order to find electric fields at the defects, we must constitute a way to excite the defect modes. Here we consider that the EM field propagates from the left along the waveguide, interacts with the nonlinear defects, reflects back, and transmits to the right. Then the transmission process can be described by the CMT stationary equations[29–31] for the even mode amplitude A_s and the odd mode amplitude A_a,

$$\begin{aligned} &\left[\omega - \omega_s - \lambda\omega_s\phi_s^2(I_1 + I_2) + i\Gamma\right]A_s \\ &\quad - \lambda\omega_0\phi_s\phi_a(I_1 - I_2)A_a = i\sqrt{\Gamma}E_{\text{in}}, \\ &-\lambda\omega_0\phi_s\phi_a(I_1 - I_2)A_s \\ &\quad + \left[\omega - \omega_a - \lambda\omega_a\phi_a^2(I_1 + I_2)\right]A_a = 0, \end{aligned} \tag{19}$$

the subscript "in" means input amplitude, and where only the even mode is coupled with the waveguide because of the symmetry. The equivalent model is shown in Fig. 1(b). The CMT equations, in fact, are the Lippmann-Schwinger equation[32,33]

$$(\omega - \widehat{H}_{\text{eff}})\begin{pmatrix} A_s \\ A_a \end{pmatrix} = i\widehat{W}E_{\text{in}}, \tag{20}$$

where the complex matrix $\widehat{H}_{\text{eff}}$ equals

$$\widehat{H}_{\text{eff}} = \widehat{H}_0 + \widehat{V} - i\widehat{W}\widehat{W}^+, \tag{21}$$

and $\widehat{W} = \begin{pmatrix} \sqrt{\Gamma} \\ 0 \end{pmatrix}$ describes the coupling of the defect modes ψ_m with the waveguide.

The amplitudes A_s and A_a are given by inverse of the matrix $\omega - \widehat{H}_{\text{eff}}$, where the matrix elements of the effective Hamiltonian $\widehat{H}_{\text{eff}}$ in turn depend on the intensities I_1 and I_2. In order to write the equations of self-consistency for the intensities at the defects $I_j, j = 1,2$ we expand the electric field at the jth defect over eigenmodes $E(\mathbf{x}_j) = \sum_m A_m\psi_m(\mathbf{x}_j)$. In the two-level approach, the expansion takes the following form:

$$\begin{aligned} E_1 &= E(\mathbf{x}_1) = \phi_s A_s + \phi_a A_a, \\ E_2 &= E(\mathbf{x}_2) = \phi_s A_s - \phi_a A_a, \end{aligned} \tag{22}$$

where symmetry properties of the eigenmodes $\psi_m(\mathbf{x})$ were taken into account. Respectively,

$$I_1 = |\phi_s A_s + \phi_a A_a|^2, \quad I_2 = |\phi_s A_s - \phi_a A_a|^2, \tag{23}$$

which defines the equations of self-consistency after substitution into Eq. (19). In general, they are rather cumbersome. Let us, first, consider the more simple case of the isolated defects so that the overlapping u can be neglected. Then the values of the eigenmodes at the defects are equal, $\phi_s = \phi_a$. Even in that simplified case, the solution of Eqs. (19) has cardinal features different from the case of the single nonlinear defect considered in Refs. 6,7, and 9–12. These features are the result of the interference of EM flows reflected by the nonlinear defects. If $\det(\widehat{H}_{\text{eff}} - \omega) \neq 0$, the amplitudes of the mode excitement for the transmission can be easily found from

Eq. (19) as follows:

$$A_s = \frac{i\sqrt{\Gamma}E_{\rm in}[\omega-\omega_0(1+2\lambda I)]}{[\omega-\omega_0(1+2\lambda I)]^2-\omega_0^2\Delta^2+i\Gamma[\omega-\omega_0(1+2\lambda I)]},\quad A_a = \frac{i\sqrt{\Gamma}E_{\rm in}\omega_0\Delta}{[\omega-\omega_0(1+2\lambda I)]^2-\omega_0^2\Delta^2+i\Gamma[\omega-\omega_0(1+2\lambda I)]}, \tag{24}$$

where $I=(I_1+I_2)/2$ and $\Delta=\lambda(I_1-I_2)$. Here we took $\phi_s=\phi_a=1$. By substituting these solutions into Eq. (23), we obtain the following nonlinear equations of self-consistency:

$$I_1 = \frac{\Gamma E_{\rm in}^2[\omega-\omega_0(1+2\lambda I_2)]^2}{[\omega-\omega_0(1+2\lambda I_1)]^2[\omega-\omega_0(1+2\lambda I_2)]^2+\Gamma^2[\omega-\omega_0(1+2\lambda I)]^2},$$
$$I_2 = \frac{\Gamma E_{\rm in}^2[\omega-\omega_0(1+2\lambda I_1)]^2}{[\omega-\omega_0(1+2\lambda I_1)]^2[\omega-\omega_0(1+2\lambda I_2)]^2+\Gamma^2[\omega-\omega_0(1+2\lambda I)]^2}. \tag{25}$$

The solution of these equations gives the steady state for the transmission in the waveguide coupled with two nonlinear defects.

Finally, we present the transmission amplitude in the framework of the CMT:[30,31,34]

$$t = E_{\rm in}-\sqrt{\Gamma}A_s. \tag{26}$$

Here the odd amplitude A_a does not contribute to the transmission amplitude because of the symmetry.

In the forthcoming calculations, we choose the parameters of the CMT model as follows: $\omega_0=1,\Gamma=0.01$, and $\lambda=-0.01$. We consider the case of isolated defects $u=0$ and $\phi_s=\phi_a=1$ and the case of coupled defects with $u=0.01$, $\phi_s=1$, and $\phi_a=1.1$. Rigorously speaking, these values u and ϕ_s,ϕ_a correlate with each other. However, in our model case, we disregard this correlation.

IV. SYMMETRY PRESERVING SOLUTION

We start with the solution $E_1=E_2$ that preserves the symmetry. In this case the incident wave excites only the symmetric even mode A_s

$$A_s = \frac{i\sqrt{\Gamma}E_{\rm in}}{\omega-\omega_0(1+2\lambda I)+i\Gamma}, \tag{27}$$

as follows from Eq. (24), with the only resonance frequency $\omega_0(1+2\lambda I)$ and the width 2Γ. The self-consistency equation for the symmetry preserving solution $I=I_1=I_2$ simplifies

$$I\{[\omega-\omega_0(1+2\lambda I)]^2+\Gamma^2\}=\Gamma E_{\rm in}^2. \tag{28}$$

That coincides with the equation of self-consistency for the single off-channel nonlinear defect[34] and is equivalent to the equation obtained in Refs. 7 and 9–12. The solution of this cubic nonlinear equation is shown in Fig. 2 by dashed lines. The frequency behavior of the intensities inherits the linear case, as shown in the inset. With growth of the input power, the resonance frequency shifts to the left because of the nonlinear contribution $2\lambda I$, as seen from Eq. (27).

The frequency behavior of mode excitations $|A_s|$ and $|A_a|$ is shown in Fig. 3 by dashed lines. As seen from Fig. 3(a), A_s has a resonance peak. Respectively, the transmission $T=|t|^2/E_{\rm in}^2$ has a resonance dip at the frequency $\omega_0(1+2\lambda I)=\omega_0(1+2\lambda E_{\rm in}^2/\Gamma)$, as shown in Fig. 4(a) by the dashed line. The last equality follows from Eq. (28).

In Figs. 5, 6, and 7 we present the dependence of the intensities I_1,I_2, the mode amplitudes A_s,A_a, and the transmission amplitude (26) on the amplitude of incident wave $E_{\rm in}$. All quantities shown have nothing spectacular for the symmetry preserving solution.

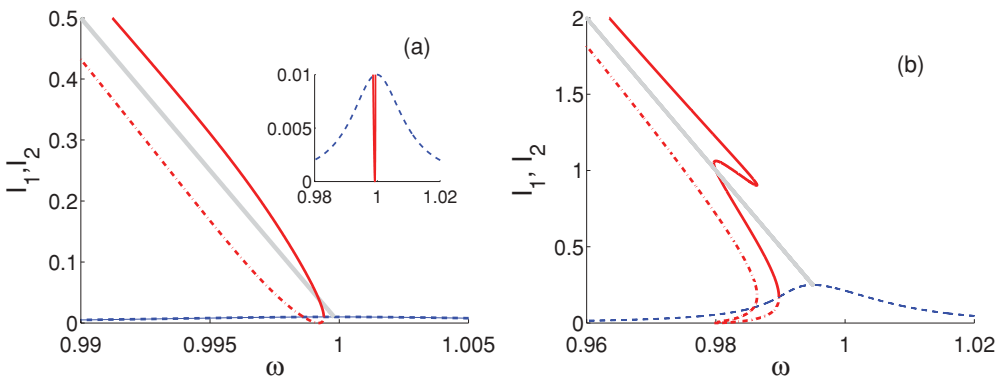

FIG. 2. (Color online) Frequency behavior of the intensities at the isolated defects $u=0$, which are the solutions of the self-consistent equation (25). (a) $E_{\rm in}=0.01$, (b) $E_{\rm in}=0.05$. Here and in the forthcoming figures, dashed blue line shows the symmetry preserving solution. Solid and dash-dotted red lines show the solutions of Eq. (25), which have different intensities at the defects I_1 and I_2, respectively. Gray thick solid line shows the third phase parity breaking solution at which $\det(\omega-\widehat{H}_{\rm eff})=0$.

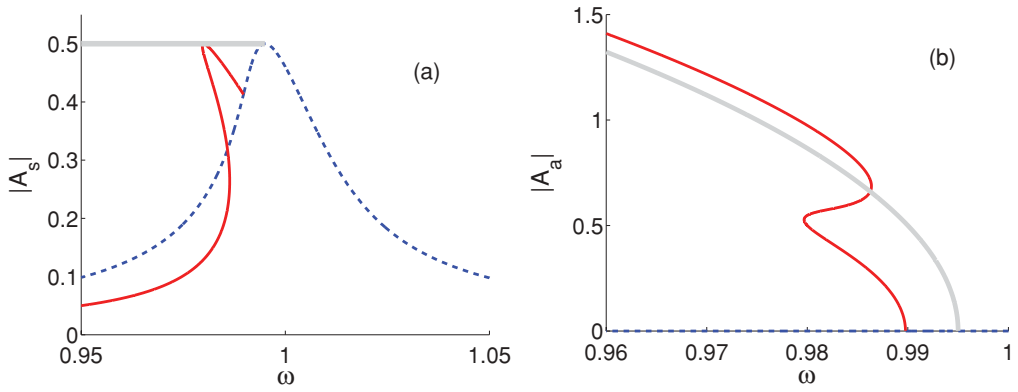

FIG. 3. (Color online) Frequency behavior of (a) the even $|A_s|$ and (b) the odd $|A_a|$ mode amplitudes of the model shown in Fig. 1(b) for $u = 0, E_{\rm in} = 0.05$. Dashed blue line shows the symmetry preserving solution, solid red line shows the symmetry breaking solution, and gray thick line shows the phase parity breaking solution.

V. SYMMETRY BREAKING SOLUTION

For the transmission through the nonlinear symmetric media, the symmetry might be broken.[14–22] Numerical solution of Eq. (19), indeed, reveals the solution with $I_1 > I_2$ [i.e., the nonlinearity gives rise to a breaking of the symmetry below (above) the critical frequency ω_c for $\lambda < 0$ ($\lambda > 0$)]. The symmetry breaking solution is shown in Fig. 2 by solid lines for I_1 and dash-dotted lines for I_2. There is also the solution that differs from the former in that $E_1 \leftrightarrow E_2$. If the solutions are stable, a choice of the solution happens incidentally, as it does for a phase transition of the second order in cooperative systems.[35] As shown in Figs. 8, 3(b), and 6(b), a value $I_1 - I_2$ or the odd mode amplitude A_a, indeed, might serve as the order parameter that characterizes the symmetry breaking.

It is easy to find a critical frequency ω_c at which the symmetry breaking solutions arise for $u = 0$ and $\phi_s = \phi_a = 1$. By substituting the relations $I_1 = I + \frac{\Delta}{2\lambda}$ and $I_2 = I - \frac{\Delta}{2\lambda}$ into Eq. (25) and substracting the intensity I_1 from the intensity I_2, we obtain

$$I\left[\left(\xi^2 - \omega_0^2\Delta^2\right)^2 + \Gamma^2\xi^2\right] = \Gamma E_{\rm in}^2\left(\xi^2 + \omega_0^2\Delta^2\right),$$
$$\left(\xi^2 - \omega_0^2\Delta^2\right)^2 + \Gamma^2\xi^2 = 4\Gamma E_{\rm in}^2\lambda\omega_0\xi, \qquad (29)$$

where $\xi = \omega - \omega_0(1 + 2\lambda I)$. By dividing these equations by each other, we obtain $\omega_0^2\Delta^2 = \xi(4\lambda\omega_0 I - \xi)$. Then we obtain the following equations for the critical value of the intensity and critical frequency for $\Delta \to 0$:

$$I_c = \frac{\xi_c}{4\lambda\omega_0}, \quad \xi_c\left(\xi_c^2 + \Gamma^2\right) = 4\lambda\omega_0 E_{\rm in}^2\Gamma. \qquad (30)$$

The second equation here defines the boundary of the symmetry breaking solution in the axes $\omega, E_{\rm in}$. If $|\xi_c| \ll \Gamma$ we have approximately

$$I_c \approx \frac{E_{\rm in}^2}{\Gamma}, \quad \omega_c \approx \omega_0 + \frac{6\lambda\omega_0 E_{\rm in}^2}{\Gamma}. \qquad (31)$$

These estimations of the critical point agree with the results of numerics given in Fig. 2.

It is surprising that there is the frequency at which the intensity at one of the nonlinear defects turns to zero as shown in Fig. 2. According to Eqs. (25) that occurs at the frequency

$$\omega_{\rm dip} = \omega_0\left(1 + 8\lambda E_{\rm in}^2/\Gamma\right). \qquad (32)$$

At this frequency we have $A_s = A_a = E_1/2 = E_{\rm in}/\sqrt{\Gamma}$ in accordance with Eqs. (24) and (22). By substituting this equality into Eq. (26) we immediately obtain that the frequency (32) defines the position of resonance dip for the symmetry

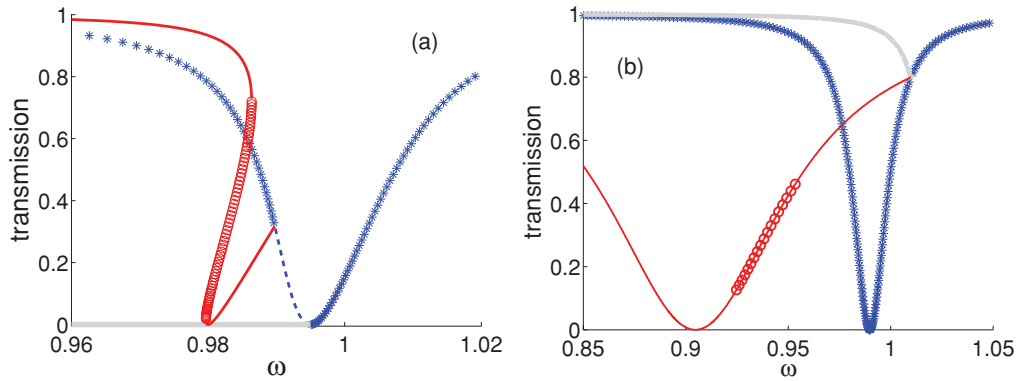

FIG. 4. (Color online) Frequency behavior of the transmission for the isolated defects (a) for $E_{\rm in} = 0.05$ and (b) for the coupled defects for $E_{\rm in} = 0.01$. Dashed blue line shows the symmetry preserving solution, solid red line shows the symmetry breaking solution, and gray thick line shows the phase parity breaking solution. Stars and open circles show stable domains of the solutions.

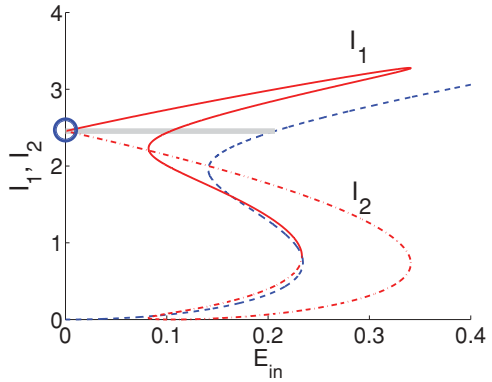

FIG. 5. (Color online) Intensities at the coupled defects as a function of E_{in} for $\omega = 0.95$. For the symmetry preserving solution (dashed blue line) and for the phase parity breaking solution (thick gray line) the intensities coincide, while for the symmetry breaking solution the intensities (solid and dash-dotted red lines) are different. The point of BSC is shown by open bold circle.

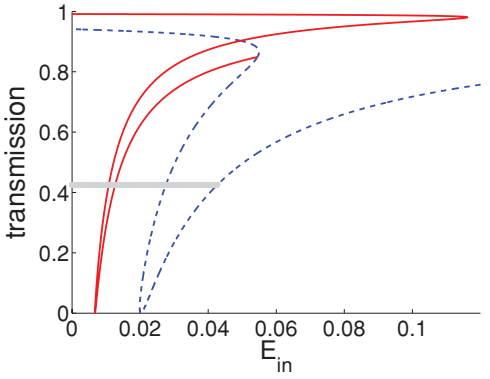

FIG. 7. (Color online) Transmission amplitude T given by Eq. (26) as a function of the input amplitude power E_{in} for the same parameters as given in the previous figure. Dashed blue line shows the symmetry preserving solution, solid red line shows the symmetry breaking solution, and gray thick line shows the phase parity breaking solution.

breaking solution. As will be shown, that result of full extinction of one of the nonlinear defects is observed in the PhC system as well [Fig. 16(b)].

In Figs. 3(a) and 3(b) we show the frequency dependence of the even and odd mode amplitudes $|A_s|$ and $|A_a|$, respectively, for $E_{\text{in}} = 0.05$. One can see that, first, the incident wave begins to excite the odd mode below ω_c for $\lambda < 0$, and, second, $|A_s|$ and $|A_a|$ show the bistability. The even mode A_s displays a resonance peak (solid line) with the resonance width twice less than the resonance width of the peak for the symmetry preserving solution (dashed line). Correspondingly, the transmission in Fig. 4 demonstrates a narrow dip for the symmetry breaking solution. In order to understand that phenomenon, let us consider the resonance poles of the even and odd amplitudes given by zeros of the denominators in Eq. (24),

$$z_{1,2} = \omega_0(1 + 2\lambda I) - \frac{i\Gamma}{2} \pm \sqrt{\omega_0^2\Delta^2 - \frac{\Gamma^2}{4}}. \qquad (33)$$

For the solution with $\Delta = 0$ we had the only resonance pole with the resonance half-width Γ. As Fig. 8 shows, there is the frequency domain roughly between 0.98 and 0.99, where $\omega_0\Delta > \Gamma/2$ and where the resonance half-width is twice less than Γ according to formula (33). Therefore, in this frequency domain we can expect the resonance dip to be twice narrower compared to the symmetry preserving solution with $\Delta = 0$.

The lesser the width of resonance, the more unstable the resonance.[1] One can thereby see that the bistability of the symmetry breaking solution is more profound in comparison to the symmetry preserving solution. The resonance peak in $|A_s|$ for the symmetry breaking solution terminates at that frequency where the odd mode amplitude $|A_a|$ arises, as seen from Fig. 3(b). Close to this frequency, the amplitude A_a has a square root behavior that is typical for the order parameter in phase transitions of the second order. The dependence of A_a on the amplitude of the incident wave demonstrates the same behavior [see Fig. 6(b)].

VI. PHASE PARITY BREAKING SOLUTION

At last, there is the solution that has equal intensities at the defects, but nevertheless a symmetry is broken because of phases of the complex amplitudes E_1 and E_2. This solution

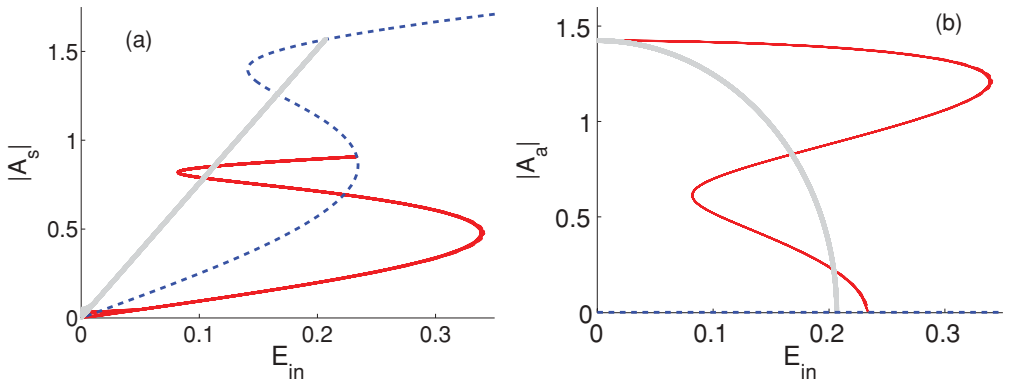

FIG. 6. (Color online) Amplitudes (a) $|A_s|$ and (b) $|A_a|$ as a function of the incident wave amplitude E_{in} for the coupled defects with the parameters $\omega = 0.95, u = 0.01, \phi_s = 1$, and $\phi_a = 1.1$. Dashed blue line shows the symmetry preserving solution, solid red line shows the symmetry breaking solution, and gray thick line shows the phase parity breaking solution.

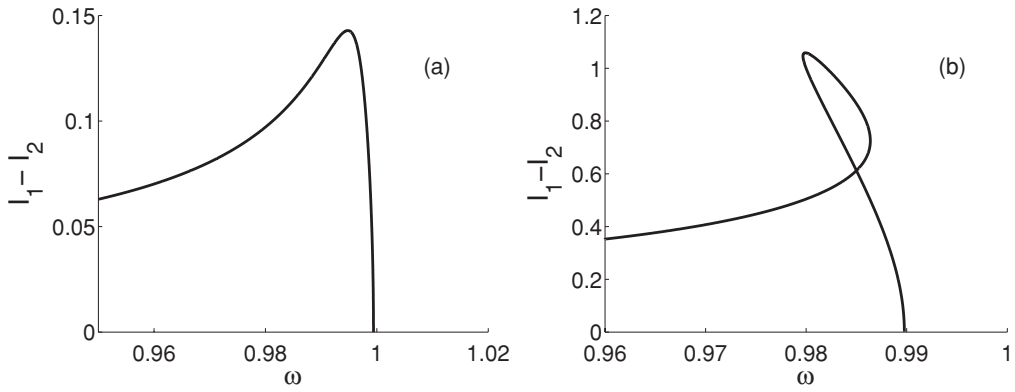

FIG. 8. Difference between the intensities of electromagnetic field intensities at the defects for $u = 0$: (a) $E_{\text{in}} = 0.01$ and (b) $E_{\text{in}} = 0.05$. Only the symmetry breaking solution is shown.

refers to the special case of Eq. (19) when the determinant of the matrix $\omega - \widehat{H}_{\text{eff}}$ equals zero (i.e., the inverse of matrix does not exist). It occurs at

$$I_1 = I_2 = I, \quad \omega = \omega_a\left(1 + 2\lambda\phi_a^2 I\right). \tag{34}$$

Then the solution of Eq. (19) exists for the even mode amplitude

$$A_s = \frac{i\sqrt{\Gamma}E_{\text{in}}}{\omega - \omega_a\left(1 + 2\lambda\phi_s^2 I\right) + i\Gamma} = \frac{E_{\text{in}}}{\sqrt{\Gamma}}, \tag{35}$$

while A_a is undetermined yet.

Let us take, for a while, the defects to be linear. Then the second equation in (34) shrinks to the isolated point $\omega = \omega_a$. As given by the CMT equations (19) and as seen from Fig. 1, this odd mode has zero overlapping with the waveguide and Eq. (34) thereby defines the bound state in continuum (BSC).[36–39] The solution of Eq. (19) $\binom{A_s}{A_a}$, with A_s given by Eq. (35) and arbitrary A_a, is therefore a superposition of the transport solution and the BSC.

For the nonlinear defects, the situation changes dramatically. First, there is the whole frequency region $\omega \geqslant \omega_a$ for $\lambda > 0$ or $\omega \leqslant \omega_a$ for $\lambda < 0$, where $\det(\omega - \widehat{H}_{\text{eff}}) = 0$ as seen from Eq. (34). Equation (34) thereby defines the BSC with eigenfrequency in whole region as dependent on the BSC intensity. Second, the BSC cannot be independently superposed to the transport solution for the nonlinear case. The BSC begins to couple with the incident wave and cannot be defined as the bound state if $E_{\text{in}} \neq 0$. We marked the BSC in Fig. 5 by the open bold circle as a single point for fixed frequency.

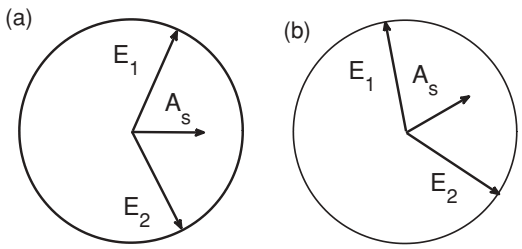

FIG. 9. Graphic solutions of (a) Eq. (36) and (b) Eq. (40), respectively. Radius of circle is $\sqrt{I}$.

A. Isolated defects

First, let the defects be isolated (i.e., $u = 0$ and $\phi_s = \phi_a = 1$). On the one hand, we obtain from Eq. (35)

$$A_s = \frac{E_1 + E_2}{2} = E_{\text{in}}/\sqrt{\Gamma}, \tag{36}$$

according to Eq. (22); that is, the even mode amplitude is constant over the frequency, as shown in Fig. 3(a) by the gray thick solid line. On the other hand, Eq. (34) directly shows that the intensities at the defects do not depend on E_{in},

$$I = \frac{\omega - \omega_0}{2\lambda}, \tag{37}$$

as shown in Fig. 5. Since $|E_1| = |E_2| = \sqrt{I}$ the only way to satisfy Eqs. (36) and (37) is to consider that the amplitudes at the defects are $E_1 = \sqrt{I}\exp(i\theta)$ and $E_2 = \sqrt{I}\exp(-i\theta)$. That is illustrated in Fig. 9(a).

With the use of Eqs. (36) and (37), we obtain

$$\cos^2\theta = \frac{2\lambda E_{\text{in}}^2}{\Gamma(\omega - \omega_0)}. \tag{38}$$

For $E_{\text{in}} \to 0$ we have the following limits: $\theta \to \pi/2, E_1 \to i\sqrt{I}, E_2 \to -i\sqrt{I}$, and $E_1 + E_2 \to 0$, as seen from Eq. (38). As soon as $E_{\text{in}} \neq 0$, the defects amplitudes are seized to oscillate in a fully antisymmetric way, as shown in Fig. 9(a). We emphasize that phase difference 2θ has nontrivial behavior if the defects are nonlinear ($\lambda \neq 0$) and the incident wave is applied ($E_{\text{in}} \neq 0$) as follows from Eq. (38). For the symmetry preserving solution $\theta = 0$ (dashed line in Fig. 10), for the symmetry breaking solution $2\theta = 0$ or π (solid line in Fig. 10), while for the present solution the phase difference 2θ behaves as an order parameter (gray thick dashed line in Fig. 10), similar to A_a shown in Figs. 3(b) or 6(b).

We define the present solution of the CMT equations (19) with the zero determinant $\det(\omega - H_{\text{eff}}) = 0$ as the phase parity breaking solution. It exists for $\omega \leqslant \omega_0 + 2\lambda E_{\text{in}}^2/\Gamma$ for $\lambda < 0$. Knowledge of the phase θ allows us now to find the amplitude of the odd mode

$$A_a = (E_1 - E_2)/2 = i\sqrt{I}\sin\theta. \tag{39}$$

The frequency behavior of the even and odd amplitudes $|A_s|$ and $|A_a|$ are shown in Figs. 3(b) and 6(b).

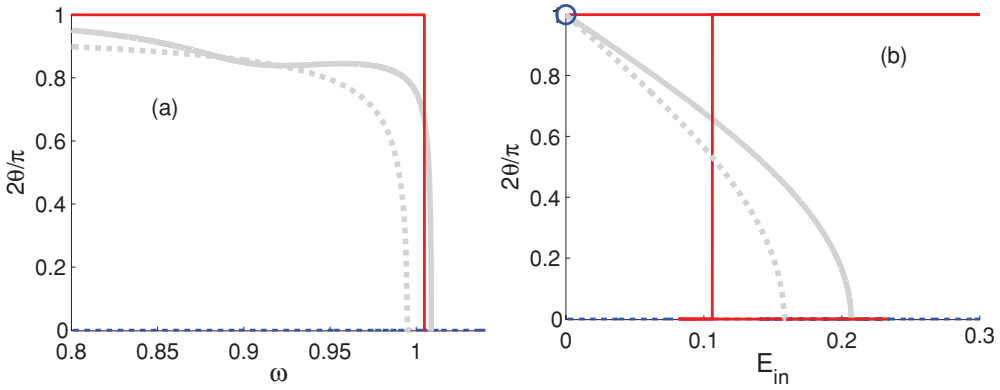

FIG. 10. (Color online) Difference between phases of the amplitudes E_1 and E_2 for $u = 0.01$ as a function of (a) the frequency for $E_{\rm in} = 0.05$ and (b) the amplitude of incident wave for $\omega = 0.95$. Dashed blue line shows the symmetry preserving solution, solid red line shows the symmetry breaking solution, and gray lines show the phase parity breaking solution, $u = 0$ dashed and $u = 0.01$ solid. The BSC point is shown by open bold circle.

Finally, by substituting Eq. (36) into Eq. (26) we obtain $t = 0$ in whole phase parity breaking solution, as shown in Fig. 4(a) by the gray thick dashed line.

B. Coupled defects

For the PhC structure shown in Fig. 1(a), the coupling between the defects u is rather small compared to the coupling between the waveguide and defects $\sqrt{\Gamma}$. Nevertheless, an account of the coupling between the defects has a principal importance, as will be seen. As was given earlier, the parameters of the coupled defects are specified as follows: $u = 0.01, \phi_s = 1$, and $\phi_a = 1.1$.

A substitution of Eq. (34) into Eq. (35) gives

$$A_s = \frac{\omega_0 + u}{\omega_0(1-\alpha) + u(1+\alpha)} \times \frac{\sqrt{\Gamma} E_{\rm in}}{\omega - \omega_r + i\Gamma_r} = \frac{A_{s0}}{\omega - \omega_r + i\Gamma_r}, \tag{40}$$

where

$$\omega_r = \frac{(1-\alpha)\omega_s\omega_a}{\omega_0(1-\alpha) + u(1+\alpha)}, \tag{41}$$

$$\Gamma_r = \Gamma \frac{\omega_a}{\omega_0(1-\alpha) + u(1+\alpha)}, \tag{42}$$

$$A_{s0} = \frac{\sqrt{\Gamma} E_{\rm in}\omega_a}{\omega_0(1-\alpha) + u(1+\alpha)}, \tag{43}$$

$\alpha = \phi_s^2/\phi_a^2$. Therefore, for the coupled defects the amplitude A_s acquires typical Bright-Wigner resonance behavior in which the nonlinearity is excluded. Respectively, a substitution of the solution (40) into Eq. (26) immediately results in the transmission having the resonance dip at the frequency ω_r with the half-width Γ_r, which depends on ratio α and u. That result is shown in Fig. 4(b) by the gray thick line. If $u \to 0, \phi_a \to \phi_s$, and $\alpha \to 1$, the frequency of the resonance dip goes away, and $\Gamma_r \to \infty$; that is, the resonance at the phase parity breaking solution disappears, and the corresponding transmission tends to zero as seen from Fig. 4(a).

Equation (34) fixes intensity at the defects

$$I = \frac{\omega - \omega_a}{2\lambda\phi_a^2\omega_a}, \tag{44}$$

which is similar to the former case given by Eq. (37). On the other hand, we have according to Eq. (22) $E_1 + E_2 = A_s/2\phi_s$, where A_s is given by Eq. (40). A graphic illustration of the solution of this equation with modules of $E_j, j = 1,2$ fixed by Eq. (44), is shown in Fig. 9(b). By presenting $E_1 = \sqrt{I}\exp[i(\beta+\theta)]$ and $E_2 = \sqrt{I}\exp[i(\beta-\theta)]$, we obtain from Eqs. (40)

$$\cos^2\theta = \frac{\lambda\Gamma_r\omega_a\omega_r E_{\rm in}^2}{2\alpha(1-\alpha)\omega_s(\omega-\omega_a)\left[(\omega-\omega_r)^2 + \Gamma_r^2\right]}, \qquad \tan\beta = \frac{\omega-\omega_r}{\Gamma_r}. \tag{45}$$

The behavior of the phase difference 2θ on the frequency or the incident wave amplitude $E_{\rm in}$ for $u = 0.01$ is shown in Fig. 10.

However, the most remarkable feature of the phase parity breaking solution for $u \neq 0$ is related to a current circulated between the defects. When the phase difference 2θ exists between two quantum dots (QD) or superconductors, connected by a weak link, a tunneling or Josephson current $J = J_0 \sin 2\theta$ will flow between them. The value of the current J_0 is proportional to the coupling constant between QDs or superconductors.[40] In order to explicitly write the expression for a current flowing between defects, we use the Green function approach developed in Refs. 6,9, and 41 for the 2D photonic crystal (PhC) of dielectric rods with the dielectric constant ϵ_0. The PhC holds the 1D cavity (waveguide) and two 0D cavities (nonlinear cavity rods) as shown in Fig. 1(a). Then the dielectric constant of full system $\epsilon(\mathbf{x})$ is a sum of periodic perfect PhC and cavity-induced terms $\epsilon(\mathbf{x}) = \epsilon_{\rm PhC}(\mathbf{x}) + \delta\epsilon(\mathbf{x}|E)$, where $\delta\epsilon(\mathbf{x}|E) = \epsilon_W(\mathbf{x}) + \epsilon_d(\mathbf{x}|E)$ is contributed by the waveguide and the two nonlinear cavities:

$$\epsilon_d(\mathbf{x}|E) = \epsilon_W \sum_{n=-\infty}^{\infty} \theta(\mathbf{x} - \mathbf{x}_n) + \sum_{j=1,2} \epsilon_j. \tag{46}$$

Here $\theta = 1$ inside the cavity rod and $\theta = 0$ outside, and the nonlinear contributions ϵ_j are given by Eq. (16). Then the

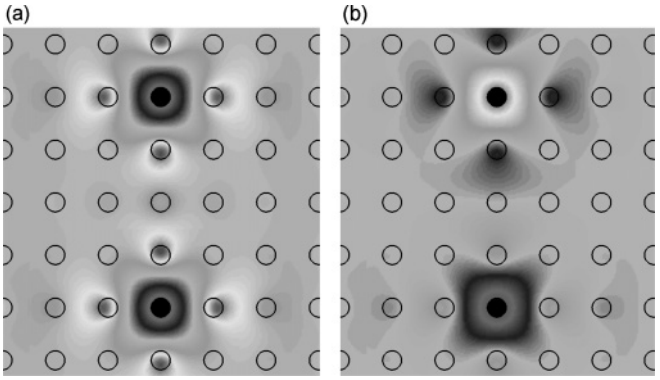

FIG. 13. Even (a) and odd (b) modes of two overlapped linear defects in PhC. The defects have the same radius as the radius of rest rods but different dielectric constant $\epsilon_0 = 3$. Then the isolated defect has the frequency of monopole mode equal to 0.3593 in terms of a value $2\pi c/a$. For the case of two defects shown here, the frequency is split to be equal to 0.3603 (even) and 0.3584 (odd).

stability are presented in Fig. 4, which shows that the stability of the phase parity breaking solution appears if only the defects are coupled and $\phi_s \neq \phi_a$. We collected the results of stability of all three solutions in Fig. 12 in the form of phase diagrams in plane of the incident wave amplitude and the frequency. One can see that the phase parity breaking solution is stable in some small area of the phase diagram.

VIII. NUMERICAL CALCULATIONS IN PHOTONIC CRYSTAL

In what follows we take the PhC as shown in Fig. 1(a) with the following parameters: The lattice constant $a = 0.5$ μm; the cylindrical dielectric rods have radius $0.18a$ and dielectric constant $\epsilon = 11.56$ (GaAs at the wavelength 1.5 μm) in air. Removing a row of rods fabricates the PhC waveguide with effective width of the order of a few a.[1,27,43] The waveguide supports a single band of guided TM mode spanning from the bottom band edge 0.315 to the upper one 0.41.[27]

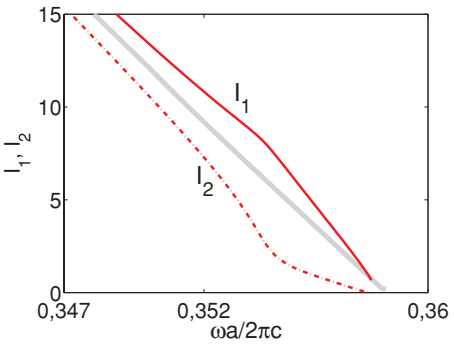

FIG. 14. (Color online) Self-consistent solution for the intensity of the EM field at the nonlinear defects in the PhC structure shown in Fig. 1(a). The symmetry preserving solution is not shown. Solid and dash-dotted red lines show the symmetry breaking solution. Gray thick solid line shows the phase parity breaking solution. The parameters of the PhC and defects are given in Fig. 13. The input power per length equals 100 mW/a. $n_2 = 2 \times 10^{-12}$ cm$^2/W$,$\lambda = -0.009$.

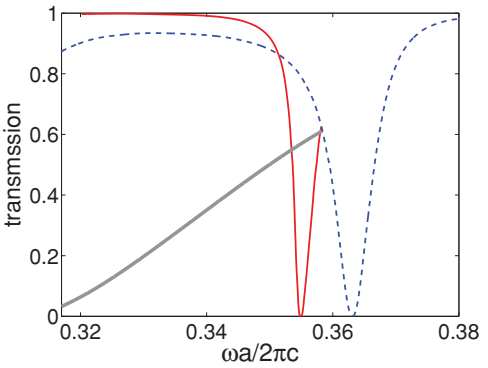

FIG. 15. (Color online) Transmission spectra in the PhC structure shown in Fig. 1(a). Dashed blue line shows the symmetry preserving solution, solid red line shows the symmetry breaking solution, and gray thick line shows the phase parity breaking solution.

We substitute two defect rods with dielectric constant $\epsilon_0 = 3$ and the same radius as shown in Fig. 1(a). We numerically solve the Maxwell equations (1) for the TM mode in the PhC with defect rods by expansion of electromagnetic field over maximally localized photonic Wannier functions.[27,33,44] For the case of isolated defects their eigenfrequency $\omega_0 = 0.3593$ where the frequency is given in terms of $2\pi c/a$. Overlapping of the defect's monopole modes gives rise to splitting of this frequency $\omega_s = 0.3603, \omega_a = 0.3584$ as numerical computation of Eqs. (1) gives. Respectively, we obtain that the value of coupling $u = -0.001$. The corresponding even and odd modes for the nearest distance a between defects were found in Ref. 45. For more distance $4a$ they are shown in Fig. 13. By

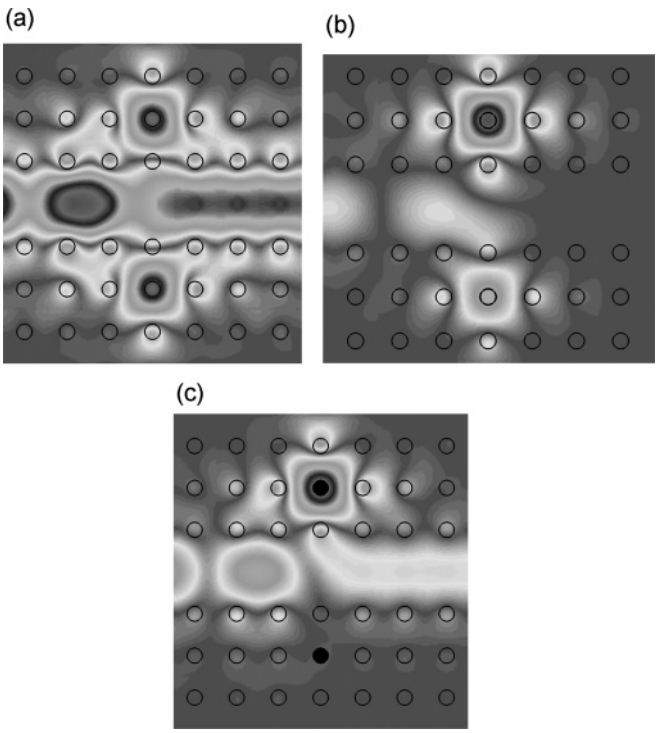

FIG. 16. Absolute value of the EM field solution for (a) the symmetry preserving solution $\omega a/2\pi c = 0.355$, (b) the symmetry breaking solution $\omega a/2\pi c = 0.355$, and (c) $\omega a/2\pi c = 0.358$. The EM wave incidents at the left of the waveguide.

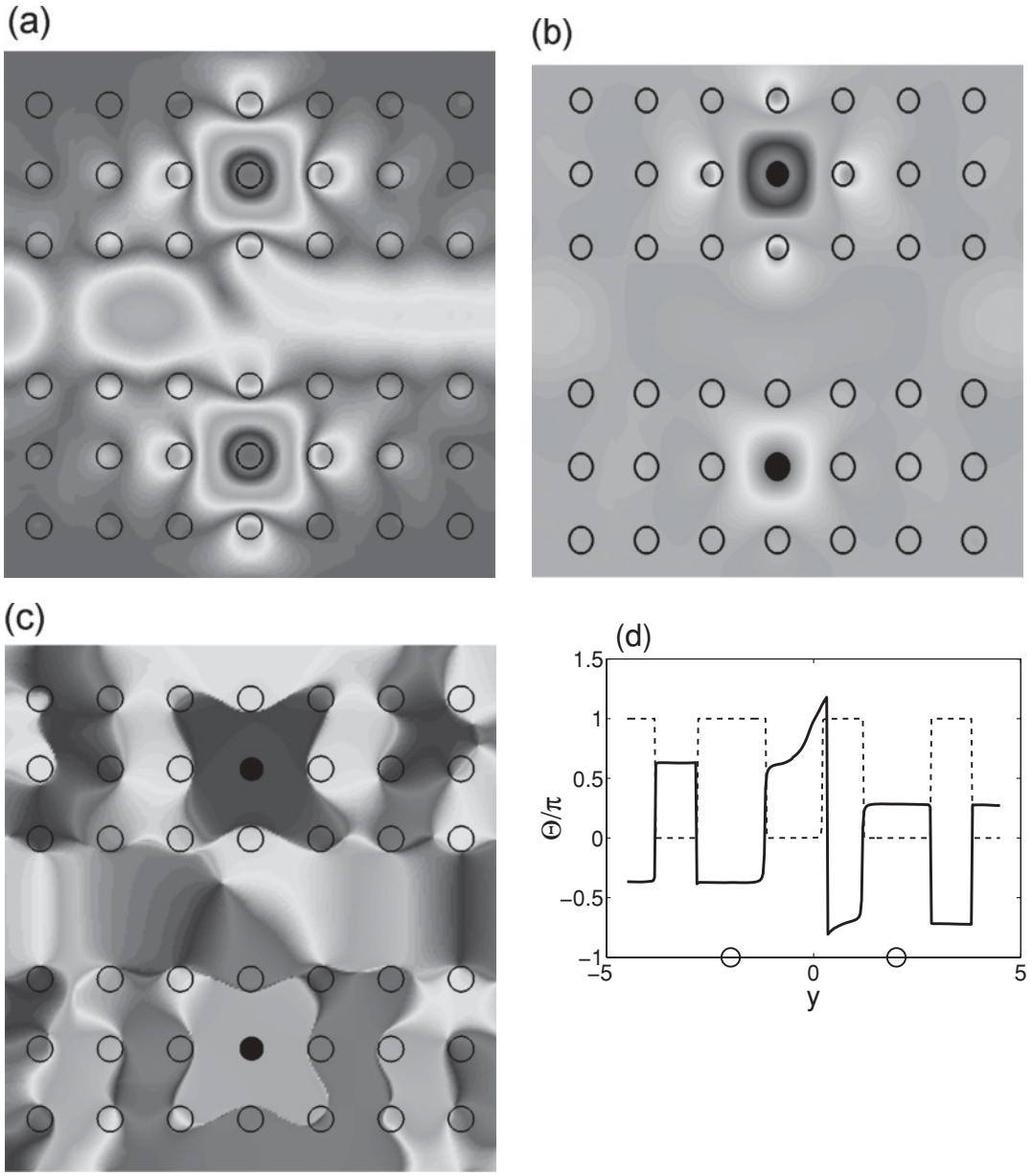

FIG. 17. Absolute value (a), real part (b), and phase $\Theta(x,y)$ (c) of the EM field for the phase parity breaking solution shown in Fig. 14 by gray line for $\omega = 0.358$. (d) Slices of the phase $\Theta(x,y)$ at $x = 0$ are given for the symmetry breaking solution (dashed line) and for the phase parity breaking solution (solid line). Positions of the defects are shown by solid open circles at bottom. The EM wave incidents at the left of the waveguide.

the normalization condition (8) the heights of the amplitude modes at the defects equal $\phi_s = 0.5569, \phi_a = 0.6179$. Let us evaluate the dimensionless nonlinearity constant λ. We take, in numerical calculations, the incident power per length of order 100 mW/a, which corresponds to the incident intensity $I_0 = 100\ \mathrm{mW}/a^2$. For a chosen PhC lattice with period $a = 0.5\mu$m we obtain that the incident intensity equals $0.04GW/\mathrm{cm}^2$. The optical Kerr effect introduced by formula (16) is described by the nonlinear refractive index n_2 for linearly polarized light[46,47] $n = n_0 + n_2 I$, where n_0 is the linear refractive index and I is an intensity of light. With the use of $\epsilon = \epsilon_0 + 2\sqrt{\epsilon_0} n_2 I$, we obtain

$$\lambda = -2\sqrt{\epsilon_0} n_2 I_0, \tag{54}$$

where σ is the cross section of the defect rods. We take the linear and nonlinear refractive indexes of the defect rods to be, respectively, $n_0 = \sqrt{\epsilon_0} = \sqrt{3}$, and $n_2 = 2 \times 10^{-12}\mathrm{cm}^2/W$. By substituting all of these estimates into (54) we obtain $\lambda \sim -0.9 \times 10^{-2}$, which is close to that used in the CMT consideration. Finally, we estimate the coupling of the defect mode with the propagation mode of the PhC waveguide $\sqrt{\Gamma}$. There are many ways to calculate Γ using, for example, Refs. 5,48, and 49. In the present paper we estimated Γ numerically by using the following approach. We took the single linear defect aside the PC waveguide, as shown in Fig. 1(a), and calculated the transmission spectra. By the resonance width of the spectra we evaluated $\Gamma = 0.00185$.

The procedure of the self-consistency for the PhC with nonlinear defects is described in Ref. 34. The solutions are presented in the form of the intensities in Fig. 14, which are similar to the CMT results shown in Fig. 2(a). Also, one can see three solutions in the transmission shown in Fig. 15, as was found in the CMT model for the transmission shown in Fig. 4. However, there is no full resonance dip predicted by the CMT for the phase parity breaking solution shown in Fig. 4 by the gray line. The left edge of the propagation band in the PhC waveguide at $\omega = 0.315$ terminates this phase resonance dip, as seen from Fig. 15. In the next figures we show patterns of the electric field component $E(x,y)$ of the TM mode in fragments of the PhC with the waveguide and the defects included. Figure 16 shows the EM field (the absolute value of the electric field) for the symmetry preserving solution (a) and for the symmetry breaking solution (b). In the latter case one can see that the field is strongly different at bottom and top. Moreover, Figs. 2 and 14 show that there is a frequency at which the intensity of the EM field might be zero at the bottom defect. Indeed, Fig. 16(c) demonstrates this case.

The phase parity breaking solution is presented in Fig. 17 by the absolute value (a), by the real part (b), and by the phase of the EM field $E(x,y) = |E(x,y)| \exp(i\Theta(x,y))$ (c). One can see that the EM intensity equals at the defects but that the real (imaginary) part of the field has different values at the defects, in full correspondence with the graphic illustration for amplitudes E_1 and E_2 in Fig. 9(b). Figure 17(d) shows the phase slice at that x where the defects are positioned. The symmetry preserving solution has no difference of phases at the defects and is not shown. One can see that the phase (dashed line) differs by π at defects for the symmetry breaking solution, while it might be any value for the phase parity breaking solution (solid line). Thus, Figs. 17(c) and 17(d) demonstrate that there is no parity relation for the phase $\Theta(x,y) = \Theta(x,-y) + \pi n, n = 0,1$ at the defects. The phase parity is broken not only at the defects in correspondence to the model theory but everywhere, including the waveguide. The EM intensity at the defects coincides, however, with an asymmetry between. Therefore, the phase parity breaking solution might be also referred to as the symmetry breaking solution, at least, in the PhC waveguide.

In agreement with the model consideration, Fig. 18 shows that current flows (the Poynting's vector patterns) are strongly different for the different solutions. For the symmetry preserving solution we have laminar current flow over the waveguide with excitation of two current vortices around each defect. The laminar flow over the waveguide and the vortical flows around defects are well separated. The whole current pattern is symmetrical relative to the symmetry transformation $y \to -y$. The picture has a similarity with ballistic electron transport in a waveguide coupled to an off-channel quantum dot.[50] For the case of the symmetry breaking solution, there is a current vortex inside the waveguide complemented by two vortices near each defect, as shown in Fig. 18(b). The circulation in vortical flow around the upper defect is opposite to the circulation around the bottom defect. Qualitatively, the current pattern is symmetrical relative to $y \to -y$; however, quantitatively, values of current are different at the defects because of the difference of the intensities of the EM field in accordance with Eq. (50). The vortical flow in the waveguide

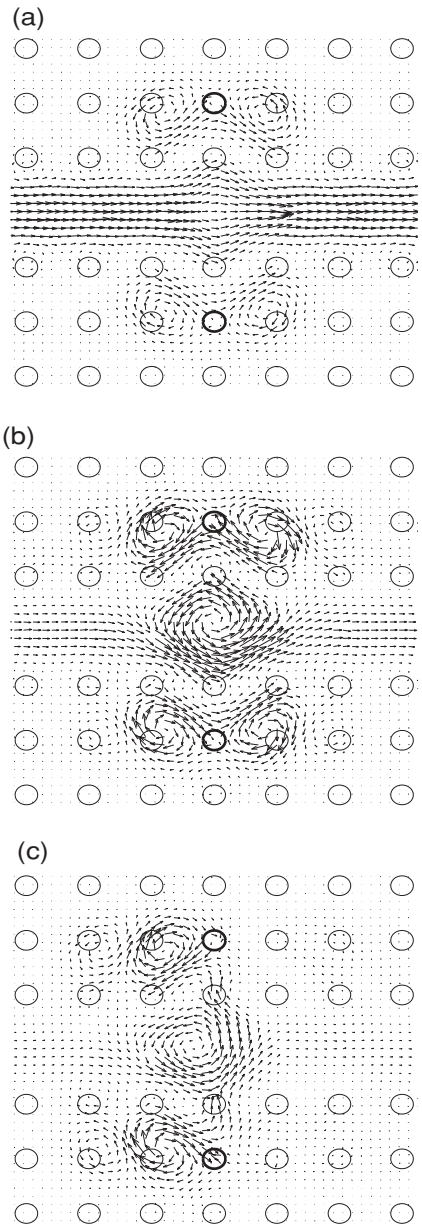

FIG. 18. Current flows for the symmetry preserving solution that inherits (a) the linear case, (b) the symmetry breaking solution, and (c) the phase parity breaking solution at $a\omega/2\pi c = 0.34$. Open bold circles mark the nonlinear defects.

and the vortical flows around the defects are well separated for both solutions. In the third case (c) for the phase parity breaking solution one can see the current vortex in the waveguide and single vortices around the defects. Moreover, one can clearly see currents flowing between the defects in correspondence to the CMT results. As a result, the flow becomes asymmetrical relative to $y \to -y$.

IX. SUMMARY AND CONCLUSIONS

Processes of transmission through a linear waveguide coupled with two nonlinear off-channel resonance cavities (defects) display a surprisingly rich variety. For the linear defects it is clear that we have a direct process of wave

transmission over the waveguide, which interferes with the backscattering processes from the off-channel defects giving rise to zeros of the transmission and the Fano resonances. As was explicitly established in Ref. 7, a nonlinearity of the defect leads to the nonlinear Fano resonance as dependent on frequency and/or incident power. For two nonlinear off-channel defects one can expect two nonlinear Fano resonances, as was found in Refs. 6,9, and 11, indeed. However, our calculations reveal a substantially more sophisticated picture of the transmission. A mathematical reason for that is the following. For the case of a single nonlinear off-channel defect, the self-consistency equation is the cubic one with total number of solutions equal to three. For the case of two nonlinear defects a complexity of two self-consistency polynomial equations of the fifth order (25) grows enormously. As a result, the number of solutions jumps up to 10. Physically, the complexity of the wave transmission in a waveguide coupled with two nonlinear off-channel defects is the result of the interference of two backscattering nonlinear processes between each other and with the direct wave transmission in the waveguide.

In order to classify the solutions we consider two cases. The first one is the case of defects that can differ by their eigenfrequencies. There is no symmetry relative to $y \to -y$. The transmission displays two resonance dips, each at the linear eigenfrequencies of the defects[12] with resonance widths determined by couplings of the eigenmodes with the waveguide. For the nonlinear case these resonances undergo shifts because of nonlinearity. If they are crossed the BSC arises, which is a discrete state with the zero resonance width.[37,38] The BSC is to have zero coupling with the waveguide and, therefore, is to be antisymmetric relative to inversion $y \to -y$. Indeed, numerics shows that the symmetry is restored in the system with two different nonlinear defects, as shown in Fig. 19 for the BSC frequency marked in Fig. 20 by the open circle. However, because of violation of the superposition principle in the nonlinear system, the incident wave couples with the BSC to give rise to a resonance of the peculiar shape shown in Fig. 20. That phenomenon is described in Ref. 13.

Surprisingly, the case of two identical nonlinear defects has more solutions. For the linear case the eigenmodes rigorously

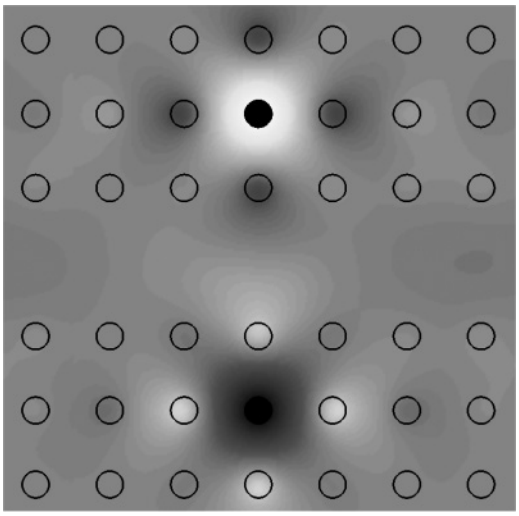

FIG. 19. Real value of the EM field for the case of different nonlinear defects for $\omega a/2\pi c = 0.3314$, the frequency of the BSC.

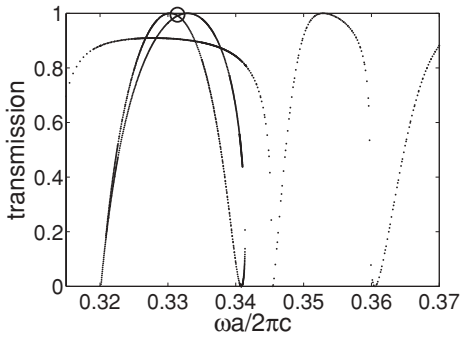

FIG. 20. Transmission spectra in the PhC structure for the case of different nonlinear defects. The parameters of the defects differ by the dielectric constants $\epsilon_0 = 2.8$ and $\epsilon_0 = 3.9$. The corresponding eigenfrequencies of the defects equal 0.3468 and 0.3622.

satisfy the symmetry $y \to -y$ (i.e., they can be classified as even and odd modes). As a result, we observe only one resonance dip at the eigensymmetric (even) mode frequency ω_s, while the antisymmetric (odd) mode does not participate in transmission phenomena because of its zero coupling with the incident symmetric wave. Therefore, that mode is obviously the BSC. The oscillations of the EM field at the defects have no phase difference: $2\theta = 0$.

For the nonlinear defects, the situation changes crucially. We have three solutions.

(i) The symmetrical solution with equal amplitudes at the defects, $E_1 = E_2$. This symmetry preserving solution inherited from the linear case exists for any frequency. There is no phase difference between EM oscillations at the defects: $2\theta = 0$. The incident wave supports only the symmetrical mode, as shown in Fig. 3. The transmission has a resonance dip at the frequency at $\omega_s(1 + 2\lambda I)$, where $\omega_s = \omega_0 - u$ is the frequency of the linear even mode, and I is the intensity of the EM field at the defects, which displays resonance enhancement.

(ii) The symmetry breaking solution for which intensities at the identical defects are not equal, $I_1 > I_2$. There is an equivalent solution in which $I_1 < I_2$. These solutions break the symmetry relative to $y \to -y$. The EM oscillations at the defects are opposite in phase: $2\theta = \pi$, although they might be in phase at some domain of the incident amplitude, as seen from Fig. 10(b). As shown in Figs. 3 and 6, the incident wave excites both symmetrical (even) and antisymmetrical (odd) modes. That results in an additional resonance dip at the frequency (32) in the transmission. At the same frequency, one of the defects becomes fully dark with zero intensity. That striking illustration of the symmetry breaking is shown in Fig. 16(c).

(iii) The phenomenon of breaking of symmetry for transmission through nonlinear system is known.[14–16,19,20] However, we reveal once more the solution in which EM oscillations at the defects have the same intensity but different phases. This difference of phases is neither zero nor π, but smoothly depends on frequency and the amplitude of the incident wave, as shown in Fig. 10. If defects are overlapped, the phase difference gives rise to current circulation between defects. The direction of current is incidental but its value is given by Eqs. (50) and (51), obtained in the framework of the tight-binding model. These model results agree with the

current flow patterns presented in Fig. 18 in application to the 2D PhC with two defect rods spaced symmetrically near the PhC waveguide.

Although the CMT equations (19) might have the steady solutions, they must be stable. As Fig. 12 shows, the domain of stability of the solution (iii) is essentially small compared to the solutions (i) and (ii). The area for the phase parity breaking solution can be expanded to increase the difference between the maximal amplitudes of the even and odd amplitudes ϕ_s and ϕ_a, as our computations show. Thus, our results reveal a surprisingly rich variety of complex dynamics of the linear PhC waveguide coupled with only two coupled nonlinear off-channel defects even in a rather simplified limit. The defects are presented by the only monopole mode, and the nonlinearity is due to the Kerr effect $\lambda|E|^2$.

ACKNOWLEDGMENTS

This work was partially supported by RFBR Grant No. 09-02-98005-"Siberia" and RFBR Grant No. 11-02-00289.

[1] J. Joannopoulos, S. G. Johnson, J. N. Winn, and R. D. Meade, *Photonic Crystals: Molding the Flow of Light* (Princeton University Press, Princeton, New Jersey, 2008).
[2] M. I. Molina and G. P. Tsironis, Phys. Rev. B **47**, 15330 (1993).
[3] B. C. Gupta and K. Kundu, Phys. Rev. B **55**, 894 (1997); **55**, 11033 (1997).
[4] M. I. Molina, Phys. Rev. B **67**, 054202 (2003).
[5] A. R. Cowan and J. F. Young, Phys. Rev. E **68**, 046606 (2003).
[6] A. R. McGurn, Chaos **13**, 754 (2003); J. Phys.: Condens. Matter **16**, S5243 (2004).
[7] A. E. Miroshnichenko, S. F. Mingaleev, S. Flach, and Yu. S. Kivshar, Phys. Rev. E **71**, 036626 (2005).
[8] S. Longhi, Phys. Rev. B **75**, 184306 (2007).
[9] A. E. Miroshnichenko and Yu. S. Kivshar, Phys. Rev. E **72**, 056611 (2005).
[10] S. F. Mingaleev, A. E. Miroshnichenko, Yu. S. Kivshar, and K. Busch, Phys. Rev. E **74**, 046603 (2006).
[11] A. E. Miroshnichenko, Yu. Kivshar, C. Etrich, T. Pertsch, R. Iliew, and F. Lederer, Phys. Rev. A **79**, 013809 (2009).
[12] A. E. Miroshnichenko, Phys. Rev. E **79**, 026611 (2009).
[13] E. N. Bulgakov and A. F. Sadreev, Phys. Rev. B **80**, 115308 (2009).
[14] B. Maes, M. Soljaĉić, J. D. Joannopoulos, P. Bienstman, R. Baets, S.-P. Gorza, and M. Haelterman, Opt. Express **14**, 10678 (2006).
[15] B. Maes, P. Bienstman, and R. Baets, Opt. Express **16**, 3069 (2007).
[16] M. Haelterman and P. Mandel, Opt. Lett. **15**, 1412 (1990).
[17] T. Peschel, U. Peschel, and F. Lederer, Phys. Rev. A **50**, 5153 (1994).
[18] I. V. Babushkin, Yu. A. Logvin, and N. A. Loiko, Quant. Electronics **28**, 104 (1998).
[19] J. P. Torres, J. Boyce, and R. Y. Chiao, Phys. Rev. Lett. **83**, 4293 (1999).
[20] L. Longchambon, N. Treps, T. Coudreau, J. Laurat, and C. Fabre, Opt. Lett. **30**, 284 (2005).
[21] K. Otsuka and K. Ikeda, Opt. Lett. **12**, 599 (1987).
[22] K. Huybrechts, G. Morthier, and B. Maes, J. Opt. Soc. A. B **27**, 708 (2010).
[23] J. Bravo-Abad, S. Fan, S. G. Johnson, J. D. Joannopoulos, and M. Soljaĉić, J. Lightwave Technol. **25**, 2539 (2007).
[24] L. D. Landau and E. M. Lifzhits, *Electrodynamics of Continuous Media* (Pergamon, Oxford, 1980).
[25] M. Skorobogatiy and J. Yang, *Fundamentals of Photonic Crystal Guiding* (Cambridge University Press, Cambridge, England, 2009).
[26] J. N. Winn, S. Fan, J. D. Joannopoulos, and E. P. Ippen, Phys. Rev. B **59**, 1551 (1999).
[27] K. Busch, S. F. Mingaleev, A. Garcia-Martin, M. Schillinger, and D. Hermann, J. Phys.: Condens. Matter **15**, R1233 (2003).
[28] P. R. Villeneuve, S. Fan, and J. D. Joannopoulos, Phys. Rev. B **54**, 7837 (1996).
[29] H. A. Haus, *Waves and Fields in Optoelectronics* (Prentice-Hall, New York, 1984).
[30] C. Manolatou, M. J. Khan, S. Fan, P. R. Villeneuve, H. A. Haus, and J. D. Joannopoulos, IEEE J. Quantum Electron. **35**, 1322 (1999).
[31] S. Fan, W. Suh, and J. D. Joannopoulos, J. Opt. Soc. Am. A **20**, 569 (2003).
[32] S. Fan, P. R. Villeneuve, J. D. Joannopoulos, M. J. Khan, C. Manolatou, and H. A. Haus, Phys. Rev. B **59**, 15882 (1999).
[33] E. N. Bulgakov and A. F. Sadreev, Phys. Rev. B **78**, 075105 (2008).
[34] E. N. Bulgakov and A. F. Sadreev, Phys. Rev. B **81**, 115128 (2010).
[35] L. D. Landau and E. M. Lifshitz, *Statistical Physics* (Pergamon, Oxford, 1980).
[36] J. von Neumann and E. Wigner, Phys. Z. **30**, 465 (1929).
[37] A. Z. Devdariani, V. N. Ostrovsky, and Yu. N. Sebyakin, Sov. Phys. JETP **44**, 477 (1976).
[38] H. Friedrich and D. Wintgen, Phys. Rev. A **32**, 3231 (1985).
[39] A. F. Sadreev, E. N. Bulgakov, K. N. Pichugin, I. Rotter, and T. V. Babushkina, in *Quantum Dots, Research, Technology and Applications*, edited by R. W. Knoss (Nova Science, Hauppauge, NY, 2008), pp. 547–577.
[40] D. R. Tilley and J. Tilley, *Superfluidity and Superconductivity* (Van Nostrand Reinhold, New York, 1974).
[41] S. F. Mingaleev, Yu. S. Kivshar, and R. A. Sammut, Phys. Rev. E **62**, 5777 (2000).
[42] N. M. Litchinitser, C. J. McKinstrie, C. M. deSterke, and G. P. Agrawal, J. Opt. Soc. Am. B **18**, 45 (2001).
[43] L.-L. Lin, Z.-Y. Li, and B. Lin, Phys. Rev. B **72**, 165330 (2005).
[44] N. Marzari and D. Vanderbilt, Phys. Rev. B **56**, 12847 (1997).
[45] S. F. Mingaleev, A. E. Miroshnichenko, and Y. S. Kivshar, Opt. Express **15**, 12380 (2007); **16**, 11647 (2008).
[46] D. C. Hutchings and B. S. Wherrett, Phys. Rev. B **50**, 4622 (1994).
[47] R. E. de Araujo and A. S. L. Gomes, Phys. Rev. A **57**, 2037 (1998).
[48] D. Michaelis, U. Peschel, C. Wächter, and A. Bräuer, Phys. Rev. E **68**, 065601(R) (2003).
[49] G. Lecamp, J. P. Hugonin, and P. Lalanne, Opt. Express **15**, 11042 (2007).
[50] P. Exner, P. Seba, A. F. Sadreev, P. Streda, and P. Feher, Phys. Rev. Lett. **80**, 1710 (1998).